Deep dive in skin structures thanks to high resolution clearing histological method

El Baraka, Oussama[1*]; Hsu, Chiung-Yueh[1]; Bilquey, Justine[1]; Gauche, Dominique[1]; Berthelemy, Nicolas[1]; Lopes Francischetti, Daniella[2]; Andre, Valerie[3]

[1] BASF Beauty Care Solutions, Pulnoy, France; [2] BASF SA, Sao Paulo, Brazil; [3] BASF Beauty Care Solutions, Lyon, France

* El Baraka, Oussama, BASF Beauty Care Solutions France, 3, rue de Seichamps, 54272 Essey-les-Nancy, France, +33-383335165, and oussama.el-baraka@basf.com

Abstract

The natural opaqueness of skin tissue and the limits of conventional histological analysis restrict the study of large structures and lack information on three-dimensional (3D) tissue visualization. The method of optical clearing was developed to increase both the probing depth of optical systems and the spatial resolution. This method allows to characterize entire tissue and can be applied to dermocosmetic research. The aim of this study was to visualize diverse 3D cutaneous models by using this new imaging methodology: coupling tissue clearing and confocal microscopy. From 6 different protocols explored, we demonstrated that an appropriate aqueous glycerol-based clearing solution could be used for in-depth visualization of immunostained 3D-spheroid dermis model, immunostained vascular network or Nile red-stained sebaceous gland structure from skin biopsies.

Keywords: Clearing; skin; confocal microscopy; high-resolution; algorithm.

Introduction.

Several *in vitro* and *ex vivo* models exist to study the skin, the most basic being monolayer cell cultures. These models are easy to set up and analyze, especially under microscopy, but lack physiological relevance. On the other hand, three-dimensional (3D) models (spheroids, skin biopsies, reconstructed skins, whole organisms, etc.) more closely mimic the body's physiology. However, these models present a challenge in terms of visualization, due to their thickness and consequent opacity.

One of the conventional solutions for observing these opaque samples is to perform successive sectioning and histological staining. However, this method is time-consuming. In addition, slicing can alter the sample, and a loss of information between slices is inevitable. What's more, slices do not allow for adequate visualization of certain structures such as networks or rare events for which it is difficult to estimate where to perform the sections [1].

To solve these problems, clearing methods have been developed to make three-dimensional samples transparent and allow whole-mount visualization without sectioning [2]. To understand the methodology of clearing methods, it is necessary to know the reasons for sample opacity.

The opacity of these thick samples is due to the phenomenon of light refraction, which occurs due to the presence of different tissue components with heterogeneous refractive indices (RI). Refraction is a physical phenomenon involving the deflection of a light wave when it encounters a medium with a different refractive index (RI). The RI is relative to the speed of light in a medium. In a biological sample, different components coexist: proteins and lipids with an RI close to 1.4, as well as cytosol and interstitial fluid with an RI close to 1.3 [3]. These differences in RI within the sample favor light refraction inducing opacity.

The purpose of clarification is to reduce light refraction phenomena, thereby increasing the transparency of processed biological samples and thus the maximum viewing depth. The

methods used to reduce light refraction are all based on the same goal: homogenization of the RI contained in the sample [3].

The various clearing methods can be divided into four main groups: simple immersion, dehydration, hyperhydration, and hydrogel coating. There is no one size fits all method as the choice depends on the scientific context [4].

Simple immersion methods consist of immersing the fixed and stained sample in a solution with an RI close to 1.4 to match proteins and lipids RI. These solutions are composed by molecules such as glycerol, 2,2-thiodiethanol (TDE), or triethanolamine and formamide (RTF) [1,5-11].

Dehydration methods include two main stages: dehydration followed by immersion in an organic clarifying solution with a high RI. Dehydration is an essential step, as it removes water and its low RI, and allows the subsequent use of hydrophobic solutions: methyl salicylate, benzyl alcohol / benzyl benzoate (BABB), dichloromethane/dibenzyl ether (DISCO), or 2,2,2,-trichloroethanol [1, 2, 12-14]. The main disadvantages of these methods are their impact on fluorescent staining and sample shrinkage [3].

Hyperhydration methods use detergents to remove lipids and urea to denature proteins, thereby reducing the average RI. In addition, the presence of urea creates an osmotic gradient that causes water to enter the sample. In contrast to previous methods, the overall RI is reduced to around 1.3, bringing it closer to cytosol RI [1]. Several hyperhydration techniques are available, such as the Sca/e method or the Sca/eS containing sorbitol, and its derivatives, [15, 4, 16] as well as the cocktails method for Clarified, Unobstructed Brain/body Imaging and

Computational analysis (CUBIC) [3, 17]. These protocols have demonstrated high efficiency, but with a potential sample expansion [1].

Embedding methods take place in three stages with at first the formation of a polyacrylamide gel in the sample to obtain a gel/sample hybrid, then delipidation by detergent as dodecyl sulfate (with or without electrophoresis to accelerate the delipidation process) and finally, the immersion in an aqueous transparency solution having a high RI. Cleared lipid-extracted acryl-hybridized rigid immunostaining/in situ hybridization-compatible tissue hydrogel (CLARITY) [18], passive CLARITY technique (PACT) and perfusion-assisted agent-release *in situ* (PARS) [19] are hydrogel-based protocols. Hydrogel coating methods often provide very effective transparency with little modifications of the structure of the samples thanks to the support created by the gel. However, the protocols are generally quite long because they are mostly dedicated to large samples such as entire organisms.

In dermocosmetic, clearing methodologies are not yet broadly used to visualize and analyze skin variations. We can cite BABB that helped evidence epidermal hyperplasia under light-sheet microscopy on skin biopsy without immunostaining in 2018 [20]. In 2019, 3DISCO was used to visualized epidermis stained by rhodamine B [21]. And in 2020, iDISCO process associated with hydrogen peroxide bleaching and immunostaining were then used to highlight differences in the spatial nerve density between 8 mm-biopsy punches from 3 facial regions [22]. However, we could also learn from physiological studies as in 2021 with Geng *et al*. [23] who compared BABB, ClearT, CLARITY and iDISCO to clarify adipose tissue punches or Christ & Jakus [24] who explored lymphatic vasculature using a modified CUBIC protocol. Regarding 3D models analysis, an interesting review of clearing methods for spheroids analysis was made by Costa *et al.* [3] and for organoids by Susaki & Takasato [15].

Consequently, as many tissue clearing methods were reported, each with different strengths and weaknesses, the aim of our study was to evaluate different protocols on dermal spheroids,

then to validate the selected method on skin tissues such as biopsies to explore vasculature, or on a large *ex vivo* pilosebaceous model previously developed [25].

Materials and Methods.

Skin models:

Skin spheroids were produced by seeding fibroblasts at 40.000 cells per well in Ultra Low Attachment 96-well culture plates and cultured in DMEM supplemented with 10% fetal bovine serum and antibiotics before centrifugation to form spheroids. A collagen boosting cocktail containing vitamin C and transforming growth factor β was used to induce synthesis and release of collagen I into the spheroids. The culture and the treatment were maintained up to 5 days in a humidified incubator at 37°C and 5% CO_2 until spheroids reached a suitable diameter to be analyzed. (250-900 µm). They were used to evaluate transparency after clearing and fibronectin and collagen type I synthesis and distribution.

Skin biopsies were prepared from abdominal skin coming from plastic surgery of informed consent donors (women, 27 and 59 yo), then rinsed in PBS buffer. They were used to evaluate the occurring vascular network.

Living pilosebaceous model was prepared as described previously [25]. Briefly pilosebaceous units (woman, face, 46 yo, informed consent) were micro-dissected from a skin sample in aseptic conditions. Epidermal, dermal and subcutaneous tissues around the pilosebacesous units were saved to maintain the architecture and cross-tissue communications. The explant samples were stabilized in 1 mL of specific medium for 1 day then incubated for 5 and 9 days at 37°C and 5% CO_2 in the presence or not of an *Epilobium angustifolium* extract at 0.017%. The culture medium was renewed every other day. The samples were used to evaluate the sebaceous gland structure in 3D and to monitor the lipid synthesis in large-scale reconstructions of 3D expression.

Fixation and staining:

Sample were fixed by 10% formalin for 30 min to 4 h according to the size of the samples then rinsed in PBS buffer. Permeation was performed using Triton X-100 in PBS. For immunostaining, antibody against collagen type I and fibronectin were used for extracellular matrix analysis, CD31 (PECAM-1) for endothelial cells, and cytokeratin 15 (CK15) for basal keratinocytes. Secondary antibodies were coupled with either fluorescein-based fluorochrome (Alexa fluor 488, green) or rhodamine-based fluorochrome (Alexa fluor 594, red) and nuclei were stained using DAPI (blue). For lipid staining, Nile red was used. Regarding permeation and immunostaining, the duration of the different steps was adjusted according to the size of the sample (from ~4.5 days for spheroids to ~10 days for biopsy)

Clearing protocols selection and validation:

Six different clearing protocols based on simple immersion, dehydration or hyperhydration principles were evaluated on dermal spheroids (protocols adapted from previously listed references). For simple immersion, different ratio of glycerol (G1 high-G2 low), increasing concentrations of 2,2′-thiodiethanol (TDE) and triethanolamine combined to formamide (RTF) have been evaluated. For hydration, the TGH-based method was applied (2,2,2-trichloroethanol, glycerol and histo-1) for dehydration, and for hyperhydration we processed AbSca/e which is a subtype of Sca/eS (urea, sorbitol, glycerol, DMSO and triton X-100). These six methods were applied on spheroids *versus* uncleared control to select the most appropriate technical solutions according to transparency and then the best one according to variations of in-depth fluorescent signals analysis. For validation on skin biopsy, the duration of glycerol G2 step was extended to 3 days.

Image acquisition, transparency and variations of in-depth fluorescent signals analysis:

Bright field images of spheroids were captured by a Leica DMi8 microscope or a screening platform for imagery (for size analysis). Images were analyzed using ImageJ or HCS Studio. To evaluate the transparency, a clarification ratio was calculated using pixel intensities of the spheroid and the background following the method described by Lallemant *et al.* [18].

For fluorescence analysis of spheroids, several equipments were used. Autofluorescence and fluorescence maintenance were first evaluated using the screening platform for imagery. For in depth visualization evaluation, high-resolution image acquisition was performed with a confocal microscope (TCS SP8, Leica) used with laser at ex. 488 nm, em.526±24 nm for fluoresceine-based fluorochrome and ex. 561 nm, em. 622±15 nm for rhodamine-based fluorochrome, and ex. 405 nm and em.450±35 nm for DAPI. According to Nürnberg *et al*. [2], to quantify the variations of fluorescent signals in depth, circular regions of interest of 200 µm in diameter were drawn at the center of the spheroid on all the acquired stacks and fluorescence of the markers (fibronectin and DAPI) was evaluated.

Regarding the skin biopsies, bright field images were acquired using a macro magnifier (Zeiss AxioZoom macroscope) and high-resolution image acquisition was also performed with a confocal (TCS SP8 or LSM780, Zeiss) or Lightsheet (Z7, Zeiss) microscope for CD31 and CK15 visualization. The 3D reconstructions were obtained from z-projections with a step of 5 µm using approximately 150 stacks. Finally, for Nile red observation in the sebaceous model, image acquisition was performed with LSM780 confocal microscope using an excitation laser at 561 nm and an emission wavelength at 598 nm. The 3D acquisition of each sebaceous gland was carried out using approximately 150 stacks with a z-step of 1.5 µm. The 3D reconstructions were obtained from z-projections on maximal intensity method. For each sebaceous gland, a digital mask was used to identify the contours of the structure to help the quantification of the sebaceous gland lipid content before quantification using a specific algorithm. The intensities of each pixel for each stack contained in the mask were averaged.

The results are expressed as the mean ratios ± SEM (n=6-8) on the untreated condition at the equivalent timepoint.

Results.

First, the sample size was maintained after the application of the six different clearing methods. Only the TGH condition seemed to slightly reduce the volume.

Clearing solutions were then evaluated according to the transparency method described by Lallemant *et al.* [11] (Figure 1). The method with the highest transparency score was Glycerol G2. This was followed by the RTF and AbSca/e or TDE methods. The methods Glycerol G1, and TGH had the lowest transparency ratios.

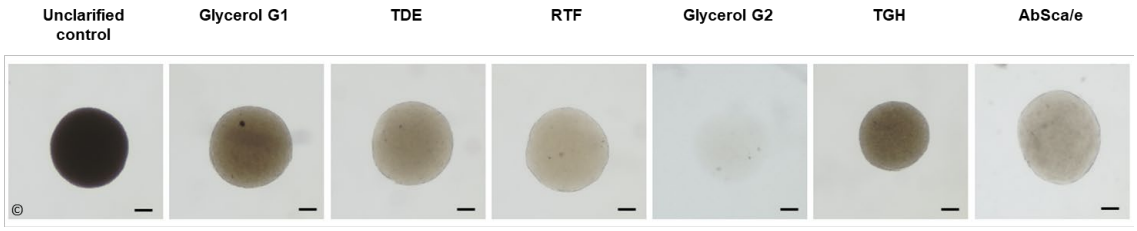

Figure 1: Illustrative pictures of the transparency observed on dermal spheroids (bright field). Six spheroids per condition were tested and confirmed on two different donors. Scale bar: 200 µm.

The final selection was performed thanks to 3 parameters: the lack of autofluorescence, the maintenance of fluorescence and the maximum depth of fluorescence visualization for fibronectin and DAPI.

Firstly, we observed some green autofluorescence when using TGH on dermal spheroids and this method was discarded. Then, as expected, without a clearing step, fibronectin and DAPI visualization was very superficial. It did not exceed 30 µm in depth as shown in Figure 2A in which a detectable signal is only observed at the sample periphery. On the other hand, all

clearing methods have demonstrated an improvement in the depth accessible for observation. However, among these methods, the glycerol G2 condition offered a significant and higher efficiency (data not shown). With a detectable signal up to 250 µm for fibronectin and DAPI, the G2 glycerol protocol provided a significantly larger area available for analysis as shown in Figure 2B. Therefore, the evaluation of fibronectin or collagen type I spatial repartition was facilitated using clearing with Glycerol G2 on dermal spheroids. Ultimately, by considering a larger portion of the sample (up to 250 µm in depth), the precision and accuracy of the evaluation of such markers having a non-homogeneous spatial distribution was greatly improved. Moreover, it was more easily to show an induction of type I collagen in cleared dermal spheroids treated with a vitamin C / TGFβ boosting cocktail (Figure 2D) compared to untreated cleared spheroids (Figure 2C).

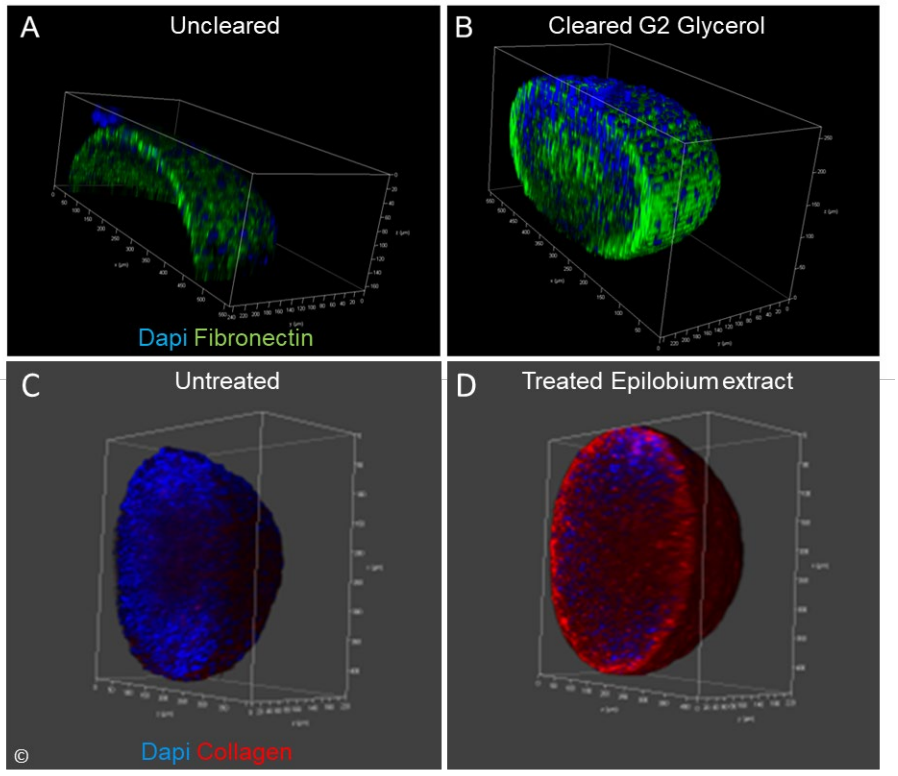

Figure 2: Illustrative pictures of Fibronectin (green)/DAPI (blue) staining in uncleared spheroid (A) or glycerol G2-cleared spheroid (B) and Collagen type I (red) /DAPI (blue) staining of untreated cleared spheroid (C) or collagen boosting cocktail treated and cleared spheroid (D).

For the following studies, efforts focused on the glycerol G2 protocol.

For vascular network evaluation, skin biopsies were used. These biopsies are 100 times larger than the previous model (dermal spheroids 0.38 mm^3; skin biopsies: 40 mm^3). The clearing protocol using glycerol G2 allowed an efficient clearing of the skin biopsy (Figure 3A) and a greater deep skin visualization of the dermal papillary plexus (Figure 3B, CD31 in green & CK15 in red)). Consequently, important structural modifications and a reduction of the vascularization network were more easily observed between young and aged donors (Figure 3C). Particularly at the level of the subepidermal area (red square area), disorganization and altered orientation of papillary capillaries may be observed in the older donor.

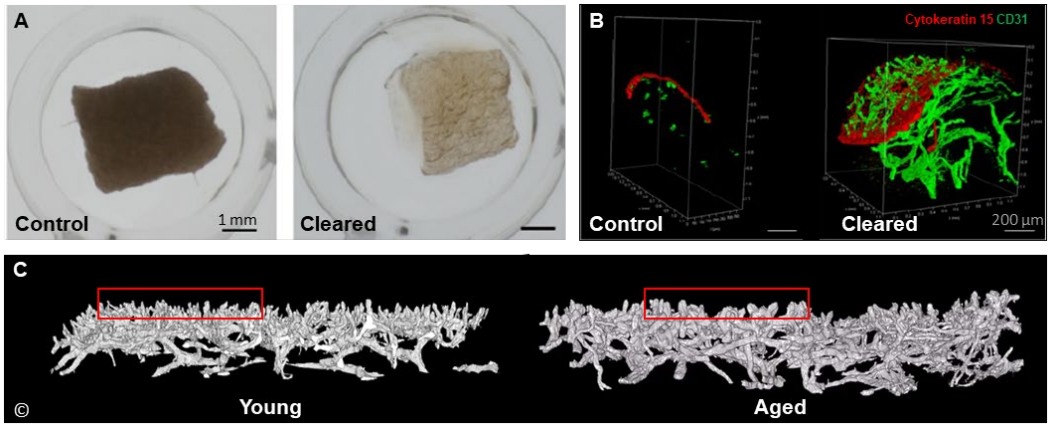

Figure 3: Illustrative pictures of A: Skin biopsy without (control) and with optical clearing (bright field); B: Immunostainings CD31 (green) and CK15 (red) on control and cleared skin biopsy; C: Dermal papillary plexus architectures of young (27 yo) and aged (59 yo) donors.

To conclude we used the selected method on a large-sized and complex but functional pilosebaceous model having received a cosmetic treatment selected on multiethnic sebocytes for its ability to reduce lipidic production. Thanks to the selected protocol applied to the skin explant samples to turn opacity of the biological tissues to transparency, we were able to

visualize *in situ* and in 3D the sebaceous glands and its lipids content when using Nile red staining (Figure 4). In the untreated control, the lipids droplets are clearly visible within the sebaceous glands. The different zone of the sebaceous gland can also be distinguished with less droplets in the proliferation zone (on the border/edge) and an accumulation of lipids in the maturation and the holocrine secretion zone. With the cosmetic treatment (*Epilobium angustifolium* extract), the sebaceous glands looked smoother, with less visible lipids droplets. The different zone of the sebaceous glands also appeared less clearly delimited. The related quantifications showed that after 9 days of culture, the lipids content was significantly reduced by 33% (SEM ± 8%; $p<0.05$) with the product at 0.017%, compared to untreated control (SEM ± 11%).

Despite the impact on lipidic production, the sebaceous gland structure described by Hou *el al*. [26] was maintained after the treatment and no impact on sebaceous gland volume was observed. This tends to evidence that the product acts on the lipid production without having any harmful long-term effect on the sebaceous gland *in vitro*.

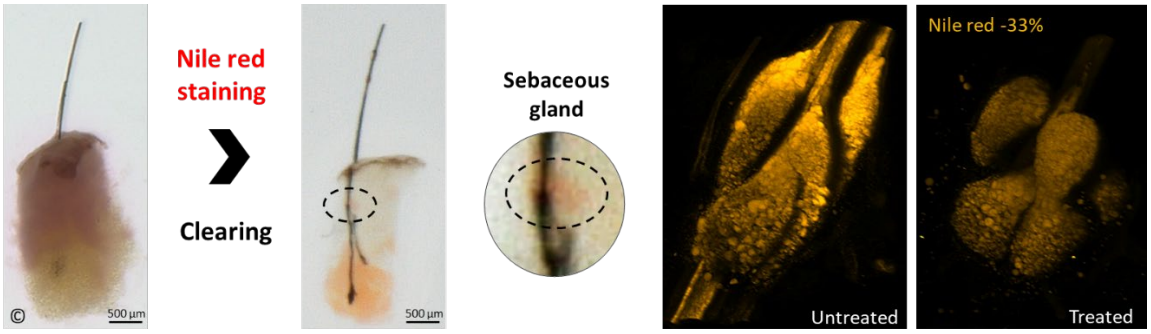

Figure 4: Human pilosebaceous unit before and after optical clearing, and effect of a treatment on Nile red staining.

Discussion.

Confocal and two-photon microscopies are usually used to perform high-resolution imaging of skin or 3D-reconstructed models of skin. The main advantage of these techniques is to enable

skin imaging in its native state without previous fixation, sectioning, or staining steps that is necessary for routine histology [27]. However, confocal, or even two-photon microscopy share similar limitations in penetration depth owing to skin opacity [28]. The main causes leading to tissue opacity are refractive index mismatch between lipid and aqueous media interfaces [18] and non-homogeneous distribution of scatterers [1], mainly lipids, collagen fibers, and myofibrils.

Tissue clearing refers to a collection of techniques that advantageously render biological samples transparent to help deep imaging of large tissue volumes [29]. Tissue clearing protocols facilitate the passage of light through a biological sample by minimizing the refractive index differences between components of the tissue [1].

For this study we aim to test easy to handle methods (easy-to-use reagents, limited time and equipment) able to preserve fluorescent immunostaining, sample size and improve in-depth visualization. Thus, we did not experiment the hydrogel embedding method.

The sample size was preserved for glycerol-based methods, TDE, RTF as previously described [8, 5, 11], or even with the hyperhydration method using Sca/eS known to induce swelling of samples [3], whereas we observed an expected limited size reduction using TGH [2].

The method which displayed the highest transparency based on clearing ratios of brightfield acquisitions was the one with a glycerol G2 solution (lower concentration). Less interesting performance was obtained with RTF (triethanolamine/formamide) and TDE (2,2′-thiodiethanol). AbSca/e method (sorbitol, glycerol, cyclodextrin, urea, triton X-100, DMSO) or TGH (trichloroethanol, glycerol, Histo-1) and glycerol G1 yielded lower transparency rates.

Regarding the important parameter of the depth visualization of the fluorescence signal, all methods increased it, although it was reduced from the edge to the center of the spheroids due

to the partial persistence of light scattering [2]. Concerning the visualization of fibronectin, the detected signal reached 30 µm for the uncleared condition. At 50 µm, best visualization is obtained first with glycerol G2, followed by AbSca/e and TGH then glycerol G1. Interestingly only glycerol G2 exhibited some fluorescence intensity up to around 250 µm. Surprisingly, in our conditions we observed some green autofluorescence with TGH.

According to these first parameters, the method glycerol G2 appeared very promising and provided staining profiles close to those obtained on cryosections for both fibronectin immunostaining and nucleic DAPI counterstaining (data not shown).

Besides, the time needed to perform the clarification process with AbSca/e complex protocol lasts 61 h, glycerol G1 48 h whereas glycerol G2 could be handled overnight (15 h), RTF in 4 h, TDE in 3 h, and TGH in 1.5 h.

According to all the results, we selected the glycerol G2 method for the later experiments. Thanks to a three-day clearing treatment due to a larger biopsy sample size compared to spheroids (100 times), we succeeded to analyze the capillary network up to 600 µm depth more easily, whereas no convenient visualization of the network was possible in uncleared condition or with successive section studies. This observation is consistent with the study published on lymphatic network using a modified CUBIC protocol on different tissues including skin [24]. Moreover, we successfully evidenced a change in the structure and repartition of the endothelial capillary network in the older biopsy as observed by Kajiva *et al.* combining iDISCO (solvent based method) for clearing Asian skin biopsy, CD31 immunolabelling and light-sheet microscopy [30]

To conclude, the selected glycerol-based clearing method was applied on a pilosebaceous model maintained up to 9 days in culture. The clearing method allowed an impressive observation of the entire sebaceous gland and Nile red-stained lipids and helped to evidence a significant lipid reduction after an *Epilobium angustifolium* extract treatment.

Conclusion.

Based on these results, the selected clearing and visualization protocol could be applied to monitor the major components of the skin and its appendages, including sebaceous gland, vascular or neuronal networks, hair follicles…Here we demonstrated that an appropriate aqueous-based clearing solution could be interestingly used for in-depth visualization of colored or immunostained skin biopsy or 3D-reconstruction. Optically cleared biopsy combined with automated algorithm analysis of confocal images now enables visualization and quantification of biomarkers or networks in larger skin compartments, appendages, both at the cellular levels and in high-resolution.

It opens new perspectives in dermatological research to study normal skin morphology, changes associated with skin conditions or dermocosmetic treatment.

Conflict of Interest Statement.

The authors are from BASF company.

References.

1. Richardson DS, Lichtman, JW (2015) Clarifying Tissue Clearing. Cell 162:246-257.
2. Nürnberg E, Vitacolonna M, Klicks J, (2020) Routine Optical Clearing of 3D-Cell Cultures: Simplicity Forward. Front Mol Biosci 7:20.
3. Costa EC, Silva DN, Moreira AF, et al (2019) Optical clearing methods: An overview of the techniques used for the imaging of 3D spheroids. Biotechnol Bioeng 116(10):2742-2763.
4. Weiss KR, Voigt FF, Shepherd DP, Huisken J (2021) Tutorial: practical considerations for tissue clearing and imaging. Nat Protoc 16(6):2732-2748.

5. Costantini I, Cicchi R, Silvestri L, et al (2019) In-vivo and ex-vivo optical clearing methods for biological tissues: review. Biomed Opt Express 10(10):5251-5267.
6. Vargas G, Chan EK, Barton JK, et al (1999) Use of an agent to reduce scattering in skin. Lasers Surg Med 24(2):133-41.
7. Kuwajima T, Sitko AA, Bhansali P, et al (2013) ClearT: a detergent- and solvent-free clearing method for neuronal and non-neuronal tissue. Development 140(6):1364-8.
8. Yu T, Zhu J, Li Y, et al (2018) RTF: a rapid and versatile tissue optical clearing method. Sci Rep 8(1):1964.
9. Ke MT, Fujimoto S, Imai,T (2013) SeeDB: a simple and morphology-preserving optical clearing agent for neuronal circuit reconstruction. Nat Neurosci 16:1154-1161.
10. Costantini I, Ghobril JP, Di Giovanna AP, et al (2015) A versatile clearing agent for multi-modal brain imaging. Sci Rep 5:9808.
11. Lallemant L, Lebreton C, Garfa-Traoré M (2020) Comparison of different clearing and acquisition methods for 3D imaging of murine intestinal organoids. J Biol Methods 7(4):e141.
12. Dodt HU, Leischner U, Schierloh A, et al (2007) Ultramicroscopy: three-dimensional visualization of neuronal networks in the whole mouse brain. Nat Methods 4:331-336.
13. Ertürk A, Bradke F (2013) High-resolution imaging of entire organs by 3-dimensional imaging of solvent cleared organs (3DISCO). Exp Neurol 242:57-64.
14. Renier N, Wu Z, Simon DJ, et al (2014) iDISCO: a simple, rapid method to immunolabel large tissue samples for volume imaging. Cell 159(4):896-910.
15. Susaki EA, Takasato M (2021) Perspective: Extending the Utility of Three-Dimensional Organoids by Tissue Clearing Technologies. Front Cell Dev Biol 14;9:679226.
16. Hama H, Hioki H, Namiki K, et al (2015) ScaleS: an optical clearing palette for biological imaging. Nat Neurosci 18(10):1518-29.

17. Susaki EA, Tainaka K, Perrin D, et al (2014) Whole-brain imaging with single-cell resolution using chemical cocktails and computational analysis. Cell 157(3):726-39.

18. Chung K, Wallace J, Kim SY, et al (2013) Structural and molecular interrogation of intact biological systems. Nature 497(7449):332-7.

19. Yang B, Treweek JB, Kulkarni RP, et al (2018) Single-cell phenotyping within transparent intact tissue through whole-body clearing. Cell 158(4):945-958.

20. Abadie S, Jardet C, Colombelli J, et al (2018) 3D imaging of cleared human skin biopsies using light-sheet microscopy: A new way to visualize in-depth skin structure. Skin Res Technol 24:294-303.

21. Fernandez E, Marull-Tufeu S (2019) 3D imaging of human epidermis micromorphology by combining fluorescent dye, optical clearing and confocal microscopy. Skin Res Technol 5:735-742.

22. Nakayama K, Sassa S, Sugiyama M, et al (2021) Three-dimensional imaging of the hyperpigmented skin of senile lentigo reveals underlying higher density intracutaneous nerve fibers. J Dermatol Sci 102(1):72-75.

23. Geng J, Zhang X, Prabhu S, et al (2021) 3D microscopy and deep learning reveal the heterogeneity of crown-like structure microenvironments in intact adipose tissue. Sci Adv 7(8):eabe2480.

24. Christ C, Jakus Z (2023) Visualization of Organ-Specific Lymphatic Growth: An Efficient Approach to Labeling Molecular Markers in Cleared Tissues. Int J Mol Sci 24:5075

25. de Bengy AF, Forraz N, Danoux L, et al (2019) Development of new 3D human ex vivo models to study sebaceous gland lipid metabolism and modulations. Cell Prolif 52(1):e12524.

26. Hou X, Wei Z, Zouboulis CC, Ju Q (2022) Aging in the sebaceous gland. Front Cell Dev Biol 10:909694

27. Aspres N, Egerton IB, Lim AC, et al (2003) Imaging the skin. Australas J Dermatol 44:19-27.

28. Imanishi Y, Lodowski KH, Koutalos Y (2007) Two-photon microscopy: shedding light on the chemistry of vision. Biochemistry 46(34):9674-84.

29. Richardson DS, Guan W, Matsumoto K, et al (2021) Tisssue Clearing. Nat Rev Methods Primers 1(1):84.

30. Kajiya K, Bise R, Commerford C, et al (2018) Light-sheet microscopy reveals site-specific 3-dimensional patterns of the cutaneous vasculature and pronounced rarefication in aged skin. J Dermatol Sci 92(1):3-5.